TECHNICAL MEMORANDUM

456

Experimental 2D-Var assimilation of ARM cloud and precipitation observations

Philippe Lopez, Angela Benedetti,
Peter Bauer, Marta Janisková
and Martin Köhler

Research Department

Submitted to Q. J. Roy. Meteor. Soc.

January 2005

European Centre for Medium-Range Weather Forecasts
Europäisches Zentrum für mittelfristige Wettervorhersage
Centre européen pour les prévisions météorologiques à moyen terme

Series: ECMWF Technical Memoranda

A full list of ECMWF Publications can be found on our web site under:
http://www.ecmwf.int/publications/

Contact: library@ecmwf.int

European Centre for Medium-Range Weather Forecasts
Shinfield Park, Reading, RG2 9AX, England

Abstract

A two-dimensional variational method (2D-Var) based on 12-hour integrations of the single column version of the ECMWF model for adjusting initial temperature and specific humidity profiles is used to identify the issues related to the assimilation of either high temporal frequency or time-accumulated observations that are directly affected by clouds and precipitation. 2D-Var experiments have been run using cloud-radar reflectivity profiles, microwave-radiometer brightness temperatures, accumulated rain-gauge measurements and total column water vapour retrievals from the Global Positioning System. All observations have been obtained from the Atmospheric Radiation Measurement Program.

In cloudy situations, it is possible to assimilate time-averaged profiles of cloud-radar reflectivities when background reflectivities are generally greater than the observations. When background reflectivities are lower than observed, the falling of the extra precipitation produced by 2D-Var hampers the convergence of the cost-function minimization. The assimilation of brightness temperatures seems more straightforward even at a half-hourly frequency.

As regards the application of 2D-Var to accumulated rain-gauge measurements, the minimization is biased towards observations that are available at the beginning of the 12-hour assimilation window, due to the reduction of precipitation sensitivities in time. However, using three-dimensional adjoint sensitivity computations, it is shown that this problem should not be as critical in four-dimensional variational assimilation (4D-Var). It is also demonstrated that the combination of precipitation data with information about the moisture field produces more realistic 2D-Var increments than with rain-gauges solely.

Finally, the implications for the future assimilation of cloud and precipitation affected observations in direct 4D-Var are presented.

1 Introduction

Over the last decade, an increasing efftort has been expended to develop new methods to utilize meteorologically useful information contained in observations of cloud and/or precipitation. Such measurements are already widely available with a large geographical coverage from various spaceborne instruments such as the Special Sensor Microwave/Imager (SSM/I), or platforms such as the Tropical Rainfall Measuring Mission (TRMM), or the AQUA satellite. Future missions, including the Global Precipitation Mission (GPM; 2010) and CloudSAT (2005), are expected to provide an even better spatial and temporal coverage and an even larger amount of information. Observations from the ground are also available from the national operational networks of precipitation radars and rain gauges, but also from several experimental sites equipped with microwave radiometers, cloud lidars and radars, such as those of the Atmospheric Radiation Measurement (ARM) Program (Stokes and Schwartz 1994).

At the same time, so-called observation operators have been designed to make the link between the atmospheric variables that are forecasted in numerical models (typically temperature, moisture, wind, surface pressure and possibly hydrometeors) and the observed quantities (radar reflectivity or brightness temperatures for instance).

Many approaches have been proposed to take this type of information into account in numerical weather prediction systems, such as nudging (Macpherson 2001), diabatic initialization (Ducrocq *et al.* 2002) and variational methods. So far, the variational treatment of cloud or precipitation-affected observations have been tested with different levels of success in various frameworks ranging from a simple one-dimensional context (1D-Var) to a complex four-dimensional environment (4D-Var). Previous works on the variational assimilation of surface rainfall retrievals from satellite include Hou *et al.* (2001), Hou *et al.* (2004) Peng and Zou (2002) , Marécal and Mahfouf (2002) and Marécal and Mahfouf (2003). Moreau *et al.* (2004) demonstrated the possibility of using multi-channel microwave brightness temperatures (TBs) from TRMM directly, in a 1D-Var context. The '1D-Var + 4D-Var' technique developed by Marécal and Mahfouf (2002) will be soon used operationally

to assimilate SSM/I TBs at the European Centre for Medium-range Weather Forecasts (ECMWF) (Moreau *et al.* 2003). In this two-step approach, a 1D-Var retrieval is first run on observed microwave TBs to produce a pseudo-observation of Total Column Water Vapour (TCWV), which is then assimilated in ECMWF's 4D-Var system.

The purpose of the present work is to investigate the feasibility of the direct assimilation of cloud and precipitation observations in a two-dimensional variational context (2D-Var), that is dealing not only with the vertical dimension as in 1D-Var but also with the time dimension. In particular, our main goal is to identify the issues related to the assimilation of such observations which are either used with a 'high' temporal resolution (e.g. 30 mn) or accumulated or averaged in time. In fact, the proposed 2D-Var framework should be seen as an intermediate stage between the simple 1D-Var approach and the much more complex (and thus more difficult to interpret) 4D-Var method. Assimilation tests to be presented here have been performed using microwave brightness temperatures (TBs), cloud-radar reflectivities, rain-gauge measurements and total precipitable water retrievals, obtained from the ARM archive.

Section 2 provides a description of each component of the 2D-Var assimilation method. The observations used in 2D-Var and their associated error statistics are detailed in section 3. The results of the assimilation experiments are presented in section 4 and the main issues they raise are discussed in section 5. Section 6 draws conclusions for the future direct assimilation of observations affected by cloud and precipitation in 4D-Var.

2 2D-Var assimilation method

The proposed 2D-Var approach involves the vertical dimension and the time dimension. It makes use of the single column version (SCM) of the ECMWF full model (see below) to depict the time evolution of the atmospheric state at a selected geographical location. The objective of 2D-Var is to find the optimal initial state of the SCM that minimizes in a least-square sense the distance between the SCM trajectory in time and a set of asynchronous observations available over a certain time window (12 hours here), given a background constraint. Figure 1 illustrates the main features of this 2D-Var approach. In the present study, two control variables are considered: temperature, T, and specific humidity, q, that are given in the form of vertical profiles. A so-called *observation operator*, H, is required to make the possibly nonlinear link between model and observations. It is composed of the SCM, denoted M, which forecasts the time evolution of the model variables, and of an operator, O, that converts the model variables into observed counterparts, translating T and q to microwave TBs, for example. M and O are detailed in the following subsection.

2.1 Observation operator

2.1.1 Single column model

The single column model version of the ECMWF model has proved to be a very useful tool for developing and testing the physical parameterizations and the vertical discretization of the equations. The idea behind the SCM approach as opposed to three-dimensional modelling of the global circulation is to eliminate the interaction between the large-scale dynamical processes and the column physics by externally specifying the large-scale dynamical terms. This requires the forcings due to horizontal advection tendencies of T, q, cloud properties, u and v, to the pressure gradient force, and to the vertical velocity. These inputs can be specified from either observations, numerical weather prediction outputs or using an idealized setup. In this study, the forcings have been specified from outputs of the ECMWF operational forecast model. Other options include (1) predicted or

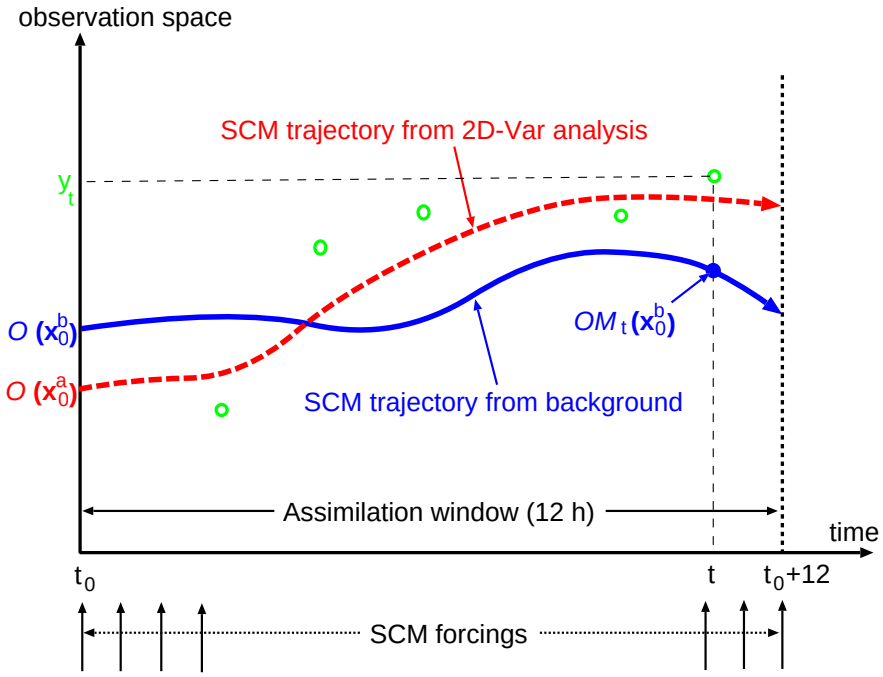

FIGURE 1: Schematic diagram of the 2D-Var assimilation method used in this study. Green dots represent individual observations. Notations are explained throughout section 2.

prescribed surface fluxes which corresponds to the activation or deactivation of the surface scheme respectively; (2) relaxation of selected state variables; and (3) specification of vertical advection tendencies instead of vertical velocity. In all experiments presented here, the surface scheme is activated, no relaxation is used, and vertical advection tendencies are specified. The SCM's discretization is written as forward in time and upwind in space, which has the advantages of stability, absence of computational mode, simplicity and convergence to the semi-Lagrangian scheme used in the 3D ECMWF model for small timesteps. The correspondence between the 60 model levels used in this study and pressure levels is described in Table 1.

The physical package used in the current ECMWF SCM corresponds to cycle 23R4. In this study however, the SCM has been run with the new simplified parametrizations of moist physical processes that were recently developed for the purpose of variational data assimilation by Tompkins and Janisková (2004) for large-scale condensation and precipitation and by Lopez and Moreau (2005) for convection. These parametrizations are used here because of their improved linearity and approximation of the nonlinear schemes used in the operational forecasts (Tiedtke 1989, 1993). It is emphasized that, in this particular framework, cloud condensate and precipitation amounts are not treated as prognostic variables.

The ECMWF SCM has been extensively used for the investigation of surface, planetary boundary layer, convection and cloud processes and their parameterization (e.g. Bechtold *et al.* 2005; Gregory 2001; Betts and Jakob 2002). The appeal of the SCM derives from its main shortcoming, namely the simplicity of removing the feedback of the subgrid-scale physical processes on the large-scale dynamics. It is also an efficient way of investigating new concepts.

2.1.2 Microwave radiative transfer model

A microwave radiative transfer model (RTM) is required to convert the model's state (temperature, moisture, cloud condensate profiles) into TBs at the frequencies of the ground-based radiometer observations (23.8 and 31.4 GHz). The calculations performed in this study rely on the assumption that no heavy precipitation is present or, in other words, that scattering can be neglected. Extinction by cloud particles, which is parametrized as in Bauer (2002), is a function of the amount of cloud liquid water and ice, of their respective permittivities and of the frequency. Therefore it does not depend on any assumed particle size distribution, which is justified for frequencies lower than 85 GHz (Bauer 2002).

2.1.3 Radar reflectivity model

The radar backscattering cross-section at 35 GHz is related to the amount of cloud and precipitating water/ice present along the radar beam. The forward modelling of this radar backscattering is performed by computing the hydrometeor optical properties. In the present version of the observational operator, all particles are assumed spherical and the Mie solution is adopted. Extinction and scattering cross-sections are calculated as functions of temperature, and integrated by assuming a Marshall-Palmer distribution for the precipitation particles and a modified-gamma distribution for the cloud particles. The radar reflectivity factor is then computed as the integral of the backscattering cross-section over the size distribution. The path-integrated attenuation is accounted for. All reflectivity and attenuation values are stored in a look-up table and classified according to the values of temperature and liquid and ice water contents, which are standard outputs of ECMWF's SCM. A bilinear interpolation is then applied to extract the reflectivity and the attenuation values corresponding to the given temperature and hydrometeor contents. The special treatment of the melting layer developed by Bauer (2001) is also included. This reflectivity/attenuation model was verified against that of Thurai *et al.* (2001) and exhibited a good consistency among the reflectivity values.

2.2 2D-Var solution

The proposed 2D-Var method searches for the model state vector at the initial time, $\mathbf{x}_0 = (T_0, q_0)$, that minimizes the following functional or *cost function*

$$J(\mathbf{x}_0) = \underbrace{\frac{1}{2}(\mathbf{x}_0 - \mathbf{x}_0^b)^T \mathbf{B}^{-1}(\mathbf{x}_0 - \mathbf{x}_0^b)}_{J_b} + \underbrace{\frac{1}{2}\sum_t (H_t(\mathbf{x}_0) - \mathbf{y}_t)^T \mathbf{R}_t^{-1}(H_t(\mathbf{x}_0) - \mathbf{y}_t)}_{J_o} \quad (1)$$

where subscript t denotes the model timestep and $\mathbf{x}_0^b$ is the background model state at the initial time. $H_t = OM_t$ is the nonlinear observation operator that converts the initial model state into observed equivalents at time t for comparison with the corresponding observations $\mathbf{y}_t$. $\mathbf{R}$ is the error covariance matrix of the observations which may be time-dependent (see section 3.2). Matrix $\mathbf{B}$ contains the background error covariances for T and q that are estimated according to Rabier *et al.* (1998). Note that T and q are assumed to be uncorrelated. An example of profiles of the background error standard deviations is given in Fig. 2. The result of 2D-Var is therefore the optimal combination of the background information (J_b) with information coming from the available observations (J_o), weighted by the inverse of their respective error covariances.

Two approaches have been tested for solving the 2D-Var problem: an iterative minimization method and a direct solver that uses the Hessian of the cost function.

In the first approach, the minimization of the functional is performed using the quasi-Newton descent algorithm (M1QN3) developed by Gilbert and Lemaréchal (1989). This requires the calculation of the gradient of the

Model level number	Pressure (hPa)
5	1
10	4
15	12
20	36
25	96
30	202
35	353
40	539
45	728
50	884
55	979
60	1012

TABLE 1: Pressure (in hPa) on every five model levels between levels 5 and 60. Values are given assuming a surface pressure of 1013.25 hPa.

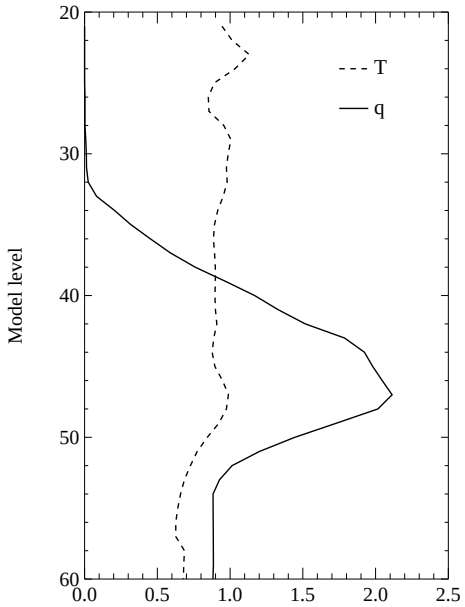

FIGURE 2: Vertical profiles of typical values of the standard deviation of the model background errors on temperature (dashed line) and specific humidity (solid line). Units are in K and g kg^{-1} respectively.

functional defined in Eq. (1) which writes

$$\nabla_{\mathbf{x}_0} J = \mathbf{B}^{-1}(\mathbf{x}_0 - \mathbf{x}_0^b) + \sum_t \mathbf{H}_t{}^T \mathbf{R}_t^{-1}(H_t(\mathbf{x}_0) - \mathbf{y}_t) \tag{2}$$

where $\mathbf{H}_t{}^T$ is the transpose (or adjoint) of the Jacobian matrix of the nonlinear observation operator, H_t. Throughout this study $\mathbf{H}_t$ has been computed using finite-differences since the tangent-linear and adjoint versions of the SCM are not available yet. It should also be noted that a preconditioning based on the left-hand square root of $\mathbf{B}$ is used to ease the minimization process.

In the alternative solving method, the second order derivative or *Hessian*, J'', of the cost function is first calculated as

$$J'' = \mathbf{B}^{-1} + \sum_t \mathbf{H}_t{}^T \mathbf{R}_t^{-1} \mathbf{H}_t \tag{3}$$

and the control vector, $\mathbf{x}_0^a$, solution of the minimization problem is then given by

$$\mathbf{x}_0^a = \mathbf{x}_0^b - J''(\mathbf{x}_0)^{-1} \nabla_{\mathbf{x}_0} J \tag{4}$$

The advantage of the Hessian method is that it yields the solution without any iteration and is therefore much cheaper computationally than the minimization with M1QN3. However, Eq. (4) relies on the assumption that the cost function is not far from being quadratic or in other words that the observation operator H is not too nonlinear, which may be sometimes far from the truth when moist processes are considered. Results from the two solving methods will be compared in section 4.1.

In the proposed 2D-Var assimilation, it is important to note that in spite of the temperature and specific humidity modifications at the beginning of the assimilation window, the SCM forcings applied at a given timestep do not vary from one iteration of the minimization to the next or when the analyzed SCM trajectory is computed. In the context of 4D-Var, the variational increments at a given grid point are spread horizontally by the structure functions (i.e. matrix $\mathbf{B}$), which implies that the changes in the horizontal gradients and therefore in the forcings due to horizontal advection remain limited. Therefore the error due to the fixed SCM forcings is likely to be small.

3 Observations

3.1 ARM dataset

All observations used in this study have been obtained from the online archive of the ARM Program (http://www.-archive.arm.gov/). The ARM Measurements are available for four geographical sites: one in Alaska, two in the Tropical West Pacific and one in Oklahoma (Southern Great Plains; SGP), for which observations date back to 1993. Here, we have used observations related to clouds and precipitation that were collected at the SGP Central Facility by a vertically-pointing microwave radiometer, a zenith-pointing millimeter cloud radar and surface rain gauges. The corresponding measured quantities are TBs in the 23.8 and 31.4 GHz channels, 35 GHz radar reflectivities and accumulated amounts of surface precipitation. The 23.8 GHz TBs are mainly sensitive to water vapour path while at the 31.4 GHz frequency they also vary with cloud liquid water path. TCWV retrievals from the ground-based Global Positioning System (GPS) network SuomiNet (Ware *et al.* 2000) have also been obtained from the ARM archive and used both either for validation or in the assimilation process. The TBs and reflectivities were averaged in time to match the model's timestep of 30 minutes.

3.2 Instrumental and representativeness errors

In order to complete matrix R involved in the variational cost function (Eq. (1)), one needs to formulate assumptions concerning the magnitude of the instrumental and representativeness errors. As for brightness temperatures, the error standard deviation is set to 1 K which accounts for the instrumental error (about 0.3 K), the error in the RTM (less than 1 K in non-precipitating conditions), and also the spatial representativeness error.

The error standard deviation for reflectivities, σ_Z, is arbitrarily set either to 2.5 dBZ or to

$$\sigma_Z = \frac{\ln(10)}{10} \left[Z_o^2 + (1.5\, Z_b)^2\right]^{\frac{1}{2}} \quad (\text{in mm}^6\ \text{m}^{-3}) \tag{5}$$

depending on whether the departures in J_o are expressed in dBZ or in mm^6 m^{-3}, respectively ($Z[dBZ] = 10\log_{10}Z[\text{mm}^6\ \text{m}^{-3}]$). Z_o and Z_b are respectively the observed and simulated background reflectivities. Note that the inclusion of the model background reflectivity in Eq. (5) is meant to avoid the specification of too small errors when Z_o is very low, which would give too much weight to the J_o term during the minimization. It also provides a crude way of taking the reflectivity model error into account. σ_Z is plotted in Fig. 3.a as a function of Z_o and Z_b.

In the case of surface precipitation assimilation, it is the square root of the rainfall amount which is used in the J_o term, since this transformation leads to an error distribution which is closer to Gaussian. Similarly to what was done for reflectivities, the error standard deviation for the square root of the surface precipitation is assumed to be given by

$$\sigma_{\sqrt{RR}} = \left[\left(0.05\ \sqrt{max(RR_o^{min}, RR_o)}\right)^2 + \left(0.10\ \sqrt{max(RR_b^{min}, RR_b)}\right)^2\right]^{\frac{1}{2}} \tag{6}$$

where RR_o and RR_b are respectively the observed and background surface precipitation amounts and where RR_o^{min}=5 mm and RR_b^{min}=0.5 mm. $\sigma_{\sqrt{RR}}$ is shown in Fig. 3.b as a function of RR_o and RR_b.

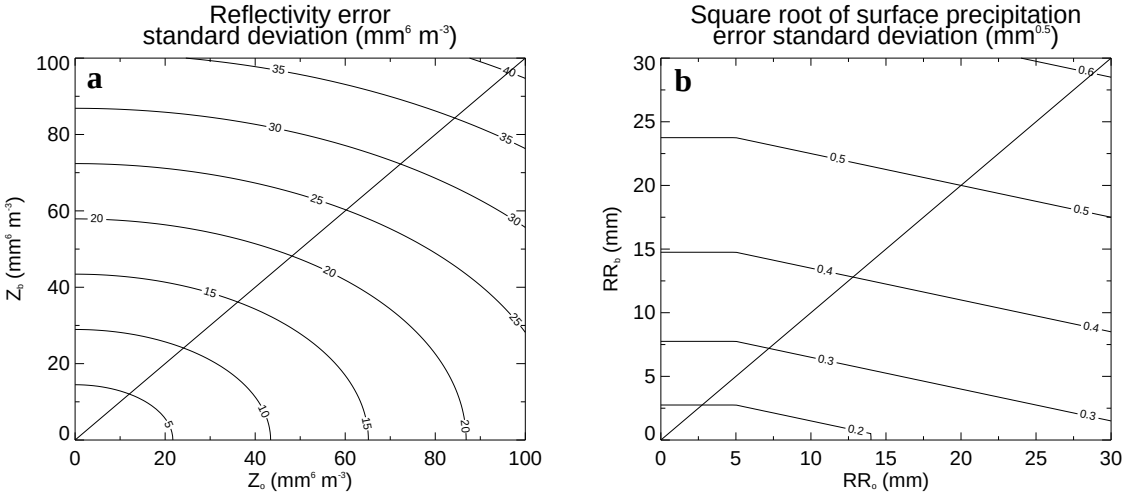

FIGURE 3: Standard deviation of the observation and representativeness error in (a) 35 GHz radar reflectivity and (b) square root of surface precipitation as a function of the observed (x-axis) and model background (y-axis) values.

Finally, the error standard deviation of the GPS TCWV retrievals has been set to 2 kg m^{-2}, which is about 30% higher than the error found in the literature (e.g. Tregoning *et al.* 1998) in order to crudely represent the forward modelling error.

3.3 Screening of observations

Given that scattering by heavy precipitation is not accounted for in our simple RTM and assuming that any wetting of the microwave radiometer sensor by surface precipitation or dew contaminates measurements, TBs observed under such conditions have been disregarded. Similarly, the reflectivity measured by the cloud radar tend to saturate in the presence of heavy precipitation, thus observations above 20 dBZ are also rejected. In other respects, large background−observation departures can be detrimental to the convergence of the minimization because they can result in a serious violation of the linear hypothesis. This turned out to be particularly true when trying to assimilate TBs and radar reflectivities. Consequently, all observations for which the absolute value of background departures are larger than 3 K for TBs and 15 dBZ for reflectivities are systematically rejected in 2D-Var. Note that a comparable screening procedure is also applied in the operational 4D-Var system.

4 Experiments

4.1 Results

4.1.1 2D-Var applied to microwave TBs and radar reflectivities

The proposed 2D-Var technique has been applied to assimilate the microwave brightness temperatures from the ground-based radiometer and reflectivities from the millimeter cloud radar in cloudy but non-precipitating situations. Earlier tests were performed using half-hourly averaged profiles of radar reflectivities alone. In these experiments, M1QN3 was not able to minimize the cost function because the discrepancies in reflectivities between the model background and the observations could be large and highly variable in both space and time. The use of too many reflectivity observations (24 timesteps $\times$ 60 levels) seemed incompatible with a successful assimilation. The problem was overcome by averaging the reflectivity profiles over the entire 12-hour assimilation window. This further averaging smooths out model−observation departures and therefore reduces the constraint imposed through the cost function. The degree to which the minimization problem is ill-posed can be assessed by studying its condition number (or ellipticity), defined as the ratio of the lowest and highest eigenvalues of the Hessian matrix of Eq. (3). Typical values of this condition number reach 4000 when trying to assimilate 30-mn reflectivity profiles but only 250 with a single profile of reflectivity averaged in time. This indicates that the ellipticity of the cost function is strongly reduced, which makes the minimization more efficient. The approach chosen here is to combine the information in the vertical provided by time-averaged reflectivity profiles with the high-temporal frequency information contained in half-hourly microwave TBs. The use of other statistical moments of reflectivities, such as their temporal variance, might help to constrain the minimization even further, but this was deemed to be beyond the scope of the present study.

The case presented here is that of a persistent stratiform high-level cloud between 0000 UTC and 1200 UTC 23 January 2001. The mean atmospheric flow was westerly with anticyclonic conditions (MSLP=1023 hPa) and with no precipitation observed at the surface. Figure 4 displays the time evolution of TCWV and microwave TBs, and also shows the time-averaged profile of reflectivity before and after the 2D-Var analysis (Hessian method) and from the observations. All quantities from the model are in better agreement with the measurements after applying the 2D-Var increments of temperature and specific humidity to the model's initial state. TBs in both channels are increased to better match the observations on average. Reflectivities are simultaneously reduced to get closer to the radar data. Although TCWV is not assimilated as such in this experiment, it is improved by 0.4 kg m^{-2} on average, leading to a better agreement with the retrievals from the radiometer and the radiosondes. This is due to the dependence of TBs on TCWV, especially at 23.8 GHz.

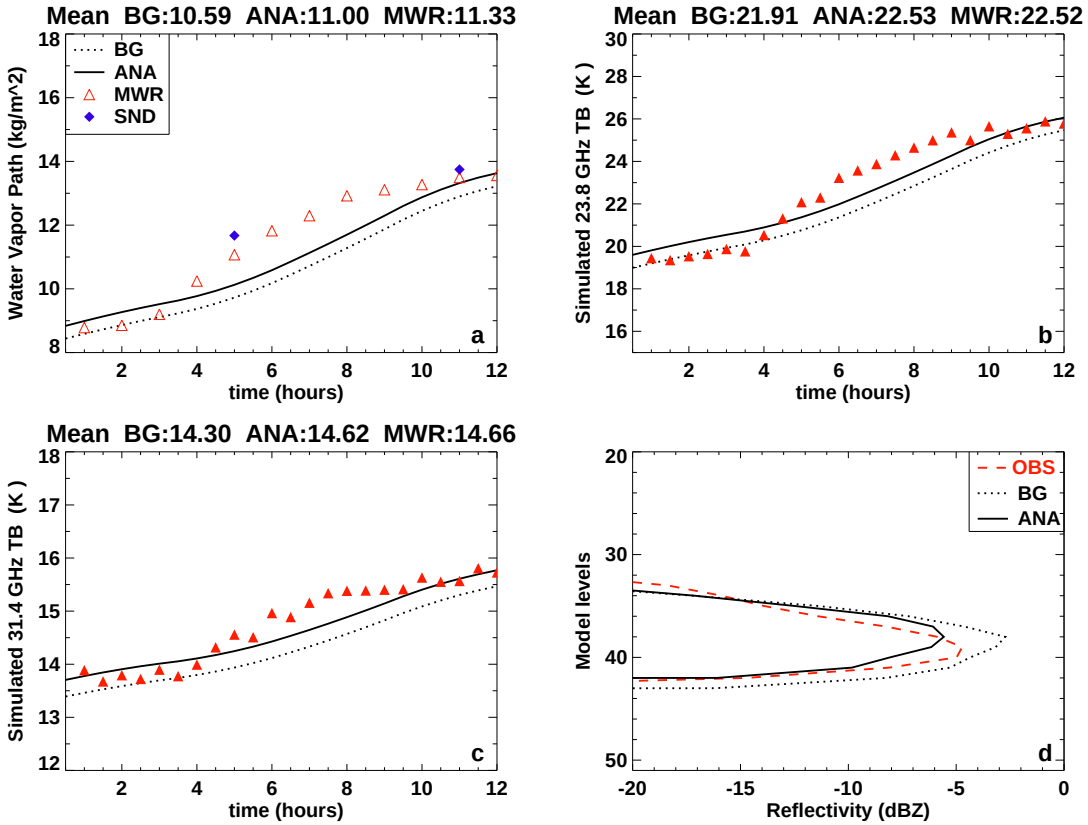

FIGURE 4: 2D-Var assimilation of half-hourly microwave TBs available over 12 hours from 0000 UTC 23 January 2001 and of the reflectivity profile averaged over the same period: 12-hour evolution of (a) TCWV, (b) 23.8 GHz TB and (c) 31.4 GHz TB as they would be measured from the ground. The averaged profile of reflectivity is displayed in panel (d). Background (BG; dotted line), 2D-Var analysis (ANA; solid line) and observations (symbols or dashed line according to panel legend) are plotted and their respective temporal average is given at the top of panels (a)-(c). MWR: microwave radiometer, SND: radiosondes. Filled triangles indicate radiometer observations that have been taken into account in the 2D-Var cost function.

Figure 5 shows the time evolution of the radar reflectivity profile before and after 2D-Var, compared to observations. Qualitatively, the overall pattern agrees rather well with the radar but quantitatively the model tends to overestimate reflectivity between 4 and 8 km above ground level, as already seen in Fig. 4.d. After 2D-Var this pattern remains unchanged but the reflectivities are in better agreement with the measurements. The corresponding increments of T and q at the beginning of the 2D-Var assimilation window shown in Fig. 6 exhibit a heating and drying out between model levels 34 and 46 that reduce the amount of scatterers (see Fig. 4.d), and a substantial moistening below model level 46 that lead to the increase of microwave TBs (see Fig. 4.b,c). The white isolines in Fig. 5.a and b indicate that although the cloud extends up to a height of 11 km, the main contribution to the simulated reflectivity comes from the larger amounts of scattering particles that are partly treated as precipitation in the model between 4 and 9 km.

This case suggests that when the model background and the observations do not differ too much and when the background reflectivity is lower than observed, 2D-Var can produce reasonably sized T and q increments at initial time that can improve both the time-averaged reflectivity profile and the time evolution of microwave TBs. However it will be shown in section 5 that in other situations the convergence of the minimization can be hampered when the simulated reflectivities need to be increased.

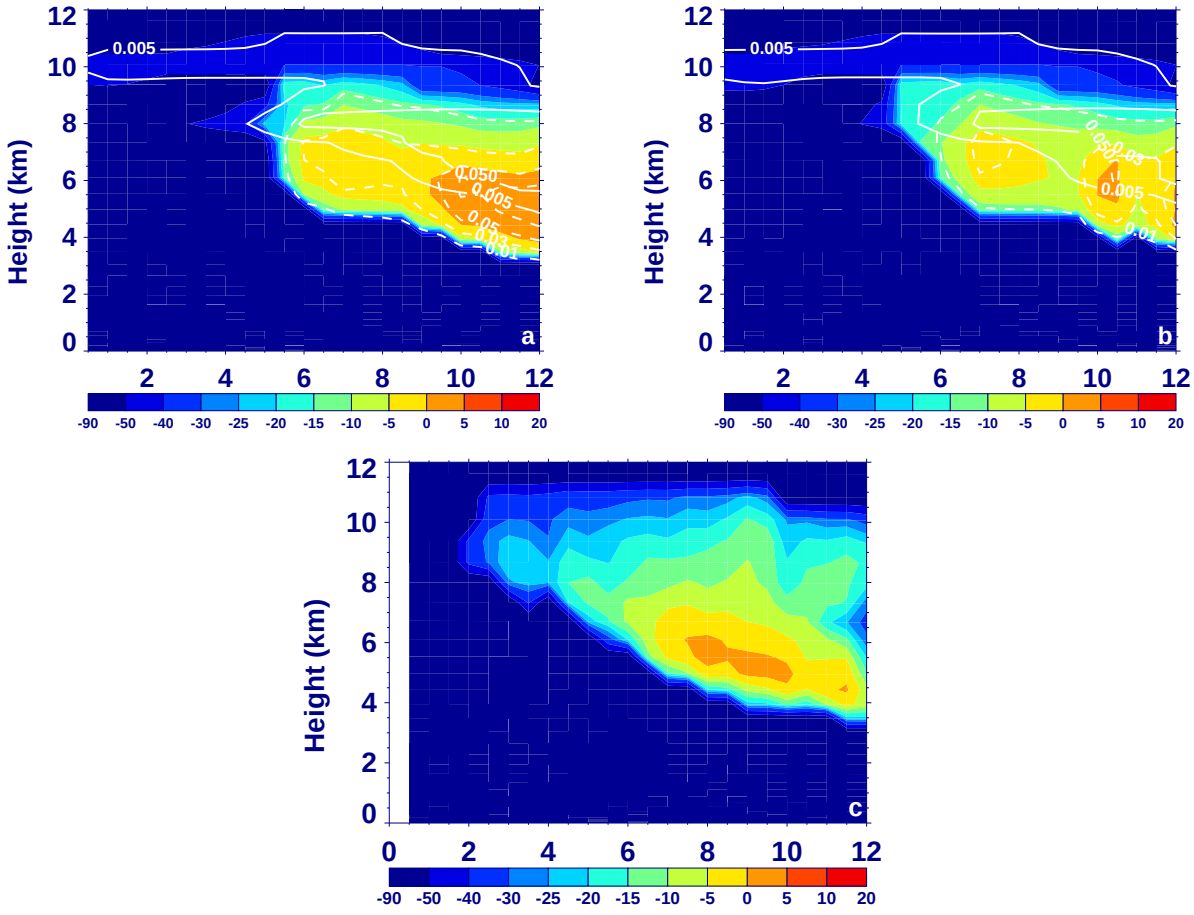

FIGURE 5: 2D-Var assimilation of half-hourly microwave TBs available over 12 hours from 0000 UTC 23 January 2001 and of the reflectivity profile averaged over the same period: 12-hour evolution of reflectivity (in dBZ) from (a) background, (b) 2D-Var analysis and (c) observations. White isolines of simulated amounts of cloud condensate (solid; g kg^{-1}) and precipitation (dash; mm h^{-1}) are also plotted in panels (a) and (b).

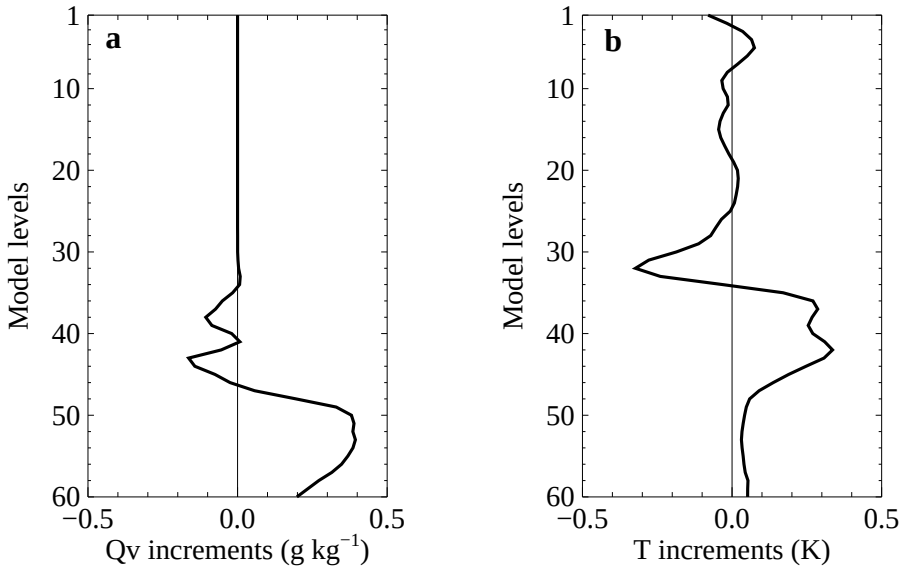

FIGURE 6: 2D-Var assimilation of half-hourly microwave TBs available over 12 hours from 0000 UTC 23 January 2001 and of the reflectivity profile averaged over the same period: increments of (a) specific humidity and (b) temperature at initial time.

4.1.2 2D-Var applied to rain gauge and GPS water vapour measurements

The 2D-Var method has also been applied to assimilate accumulated rain-gauge measurements collected at the ARM SGP site, which were also combined with GPS TCWV data in some experiments. Tests have been performed to assess the impact of the frequency of the precipitation observations in the 12-hour assimilation window and the influence of the choice of the solving method on the 2D-Var results.

Various experiments will be presented here, as summarized in Table 2.

Experiment name 24 October 2002	Solving method	Frequency of accumulated rain-gauge observations	Assimilation of half-hourly GPS TCWV retrievals
H_R1	Hessian	12h	No
H_R4	Hessian	3h	No
M_R1	M1QN3	12h	No
H_R1_GPS	Hessian	12h	Yes
H_R4_GPS	Hessian	3h	Yes

TABLE 2: Configurations of 2D-Var assimilation experiments with rain-gauge and GPS TCWV data.

First, the focus is on a non-convective rainy event that took place on 24 October 2002, with the 12-hour assimilation starting at 1200 UTC. Figure 7 displays a summary of the results of these experiments in terms of the time evolution of TCWV and accumulated surface precipitation. The corresponding analysis increments of specific humidity and temperature at initial time are plotted in Fig. 8. Figures 7 and 8 indicate that the Hessian and M1QN3 solving methods lead to very similar results. This is particularly true of the surface-rain evolution in Fig. 7.b for which the two curves are literally superimposed. Note that eight iterations were performed with M1QN3 and that the cost function dropped from 10.3 to 2.6. Figure 7.a and 8.a show that an overall reduc-

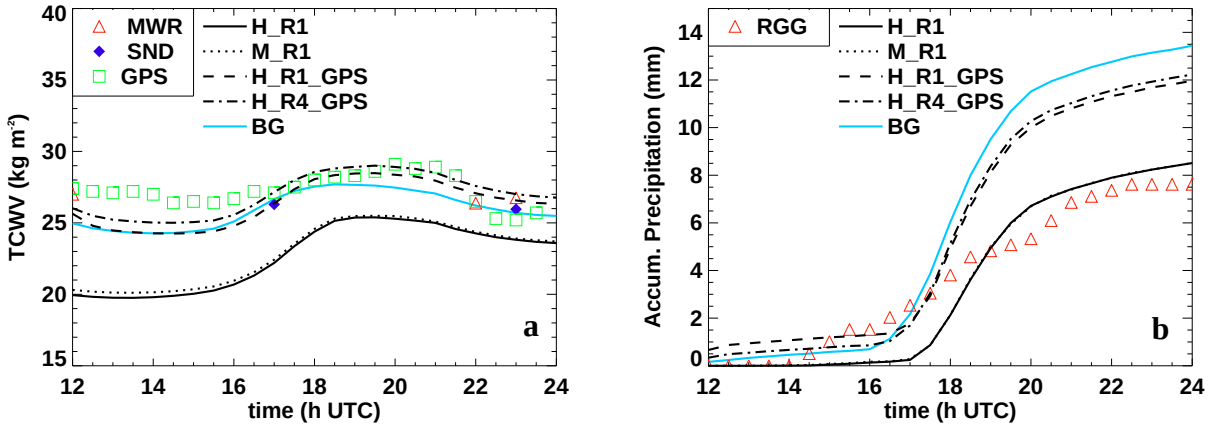

FIGURE 7: 2D-Var assimilation of accumulated rain-gauge measurements and GPS TCWV data available over 12 hours from 1200 UTC 24 October 2002. Experiments are described in Table 2. Panels (a) and (b) show the 12-hour evolution of TCWV and accumulated surface precipitation respectively, before (BG; cyan line) and after 2D-Var (experiment names indicated in legend; black lines). Available observations are shown with symbols as indicated in the legend: microwave radiometer (MWR), radiosondes (SND), GPS, and rain-gauge (RGG).

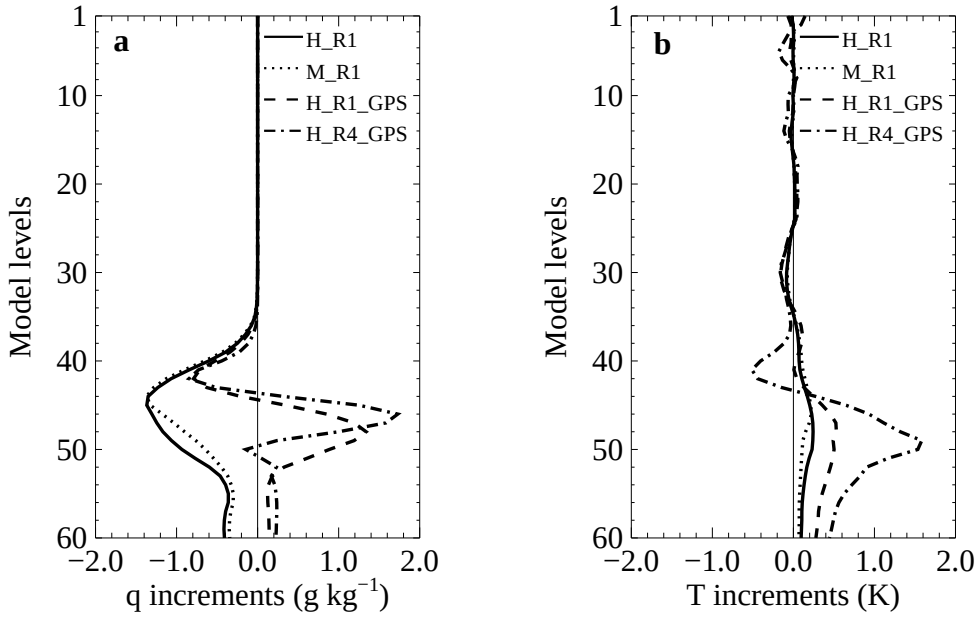

FIGURE 8: 2D-Var assimilation of accumulated rain-gauge measurements and GPS TCWV data available over 12 hours from 1200 UTC 24 October 2002. Experiments are described in Table 2. Panels (a) and (b) show the increments of specific humidity and temperature at the initial time, respectively.

tion of the moisture field is required throughout the troposphere to make the simulated 12-hour accumulated surface precipitation match the rain-gauge measurement. However, the corresponding drop in TCWV of up to 5 kg m^{-2} (Fig. 7.a) is in total disagreement with any of the consistent GPS, radiosonde and radiometer observations. Therefore, the improvement on precipitation is obtained through a degradation of the moisture field. A slight heating of less than 0.2 K implies higher values of saturation specific humidity and therefore also contributes to the decrease of simulated precipitation.

The joint assimilation of half-hourly GPS TCWV data and rain-gauge measurements provides a beneficial constraint on the humidity field during the minimization. Indeed the curves for experiments H_R1_GPS and H_R4_GPS in Fig. 7 exhibit improvements in both terms of TCWV (increased by about 1 kg m^{-2}) and surface precipitation, even though the latter field is not improved as much as it was in experiment H_R1, as expected. This implies that the assimilation of rain-gauge observations in a 4D-Var context should perform better if other types of nearby observations are available to constrain the minimization. The apparent opposite influences of rain and moisture observations in the studied case could be due to the fact that 2D-Var does not modify the dynamical fields such as vertical velocity. The inclusion of increments of vorticity and divergence in 4D-Var could eliminate this limitation, but this will need to be checked. The vertical profiles of 2D-Var increments of both T and q look very different when the GPS data are added, with a moistening and heating between the surface and model level 43, and opposite changes above. As a moistening of the lower half of the troposphere is needed to adjust the TCWV field to the GPS observations, a heating stronger than in experiment H_R1 is necessary to simultaneously reduce the amount of surface precipitation.

The comparison of the curves of experiments H_R1_GPS and H_R4_GPS shows that when four 3-hourly accumulated rainfall measurements are assimilated instead of a single 12-hourly one, the magnitude of the 2D-Var temperature increments increases. This can be explained by the larger contribution of the four precipitation observations to the J_o term.

The second case that is presented is the convective rainy event that was observed between 0000 UTC and 1200 UTC on 16 June 2002. Figure 9 displays a summary of the results of these experiments in terms of the time evolution of TCWV and accumulated surface precipitation. With a single observation of 12-hourly accu-

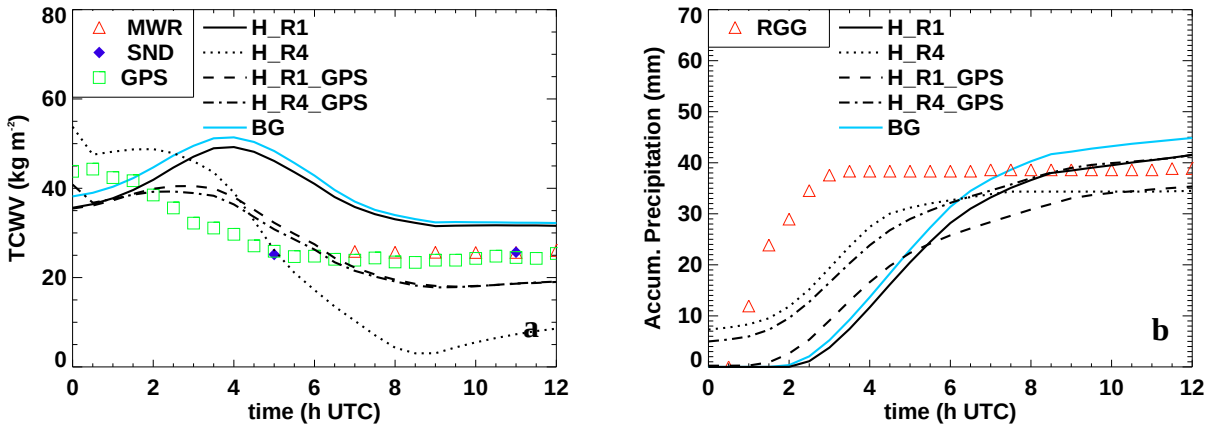

FIGURE 9: Same as in Fig. 7, but for 16 June 2002.

mulated rain at the end of the assimilation window (H_R1), 2D-var produces a slight initial drying that leads to a reduction of the background precipitation towards the measurement, but the timing of the rainfall is not significantly modified. Figure 9.a indicates that the simulated TCWV remains generally far too high compared

to the GPS, radiosonde, and radiometer data. With four 3-hourly rain observations (H_R4), a strong initial moistening of 15 kg m^{-2} is necessary to increase simulated precipitation over the first half of the assimilation window in order to improve the timing of the event. However, after 5 hours, the SCM becomes unrealistically drier than observed (Fig. 9.a) due to the earlier increase of rain production. As a result of this, the final rain accumulation after 2D-Var becomes slightly too low. When GPS TCWV data are also assimilated (H_R1_GPS and H_R4_GPS), the amount and the timing of the rainfall are both improved, especially with four rain observations. Interestingly, at the same time, Fig. 9.a shows that the SCM TCWV gets closer to the observations. This again stresses the importance of combining rain observations with measurements of the moisture field.

5 Discussion

As mentioned in section 4.1.2, some 2D-Var experiments indicated a potential limitation related to the way precipitation is treated in the model when 2D-Var is applied to vertical profiles of reflectivity. An illustration of the issue is given in Fig. 10 from a 2D-Var experiment started at 0000 UTC 4 February 2001 using either reflectivities only or reflectivities combined with half-hourly TBs. In this example some condensate of stratiform

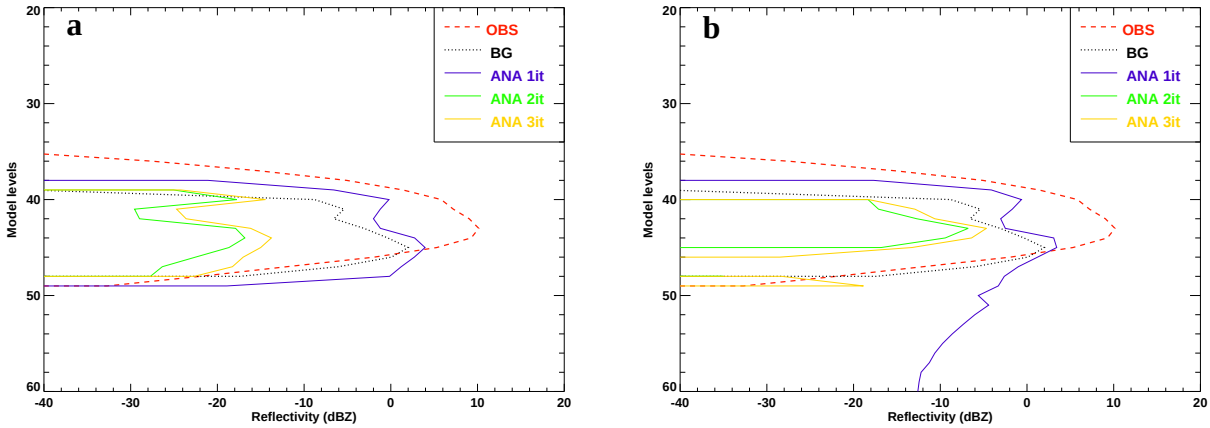

FIGURE 10: Panel (a): 2D-Var assimilation of the reflectivity profile averaged between 0000 UTC and 1200 UTC 4 February 2001: averaged profiles of reflectivity from cloud-radar observations (OBS; dashed line), prior to (BG; dotted line) and after 2D-Var analysis (ANA; solid lines) performing 1, 2 or 3 iterations using the Hessian solving algorithm. Panel (b): same as in (a), but with half-hourly microwave TBs also assimilated.

origin is seen by the cloud radar between model levels 35 and 49, with no precipitation at the ground and the freezing level around level 50. Averaged simulated reflectivities prior to 2D-Var are substantially lower than observed between levels 35 and 45, especially above level 40. After a single minimization *using the Hessian method*, the 2D-Var analyzed reflectivities are increased. This change goes in the right direction with respect to the observations above level 45 but yields far too high reflectivities below, especially when observed TBs are also assimilated. This is due to the falling of the additional precipitation produced by 2D-Var inside the cloud to match the observed reflectivities. In panel (a), most of this extra precipitation evaporates throughout the subcloud layer, while most of it reaches the surface in panel (b) due to the low-level moistening required to match observed TBs (not shown). In both cases, the new simulated reflectivities become far too high below model level 47. Similar conclusions can be drawn when M1QN3 is used to minimize the cost function (not shown). The unrealistic increase of simulated reflectivities below model level 47 is strengthened by the assumption that any precipitation produced in the model at a given level reaches the ground within one time step, which is a poor assumption for snow. If extra iterations of the Hessian solver are performed, 2D-Var reduces the simulated

reflectivities to values that become lower than the background ones and no improvement towards the observations can be reached. It is therefore important to carefully consider how precipitation is treated in the model as soon as information about the vertical structure of clouds and hydrometeors is to be assimilated. Implementing a prognostic treatment of snow based on realistic fall velocities, as in Lopez (2003), would probably help to lessen the problem substantially, but this will need to be tested.

Note that this problem did not affect the case presented in section 4.1.1 because the simulated reflectivities were initially higher and not lower than the observations. In that case, several iterations of the Hessian solver did not bring any significant change to the 2D-Var solution compared to that after a single iteration, as expected in a completely linear framework.

Another interesting issue has been found by looking at the time evolution of the surface-rainfall Jacobians throughout the assimilation window. As the Jacobians are obtained by perturbing a given variable (at initial time) on each model level separately, one can define a norm that is simply set to the maximum absolute value of the Jacobians over all levels. In Fig. 11, the norm of the Jacobians of the 3-hourly surface precipitation with respect to the initial profiles of specific humidity and temperature is found to decrease in time regularly (from experiment H_R4_GPS). This indicates that in 2DVAR the magnitude of the Jacobians is not governed by the

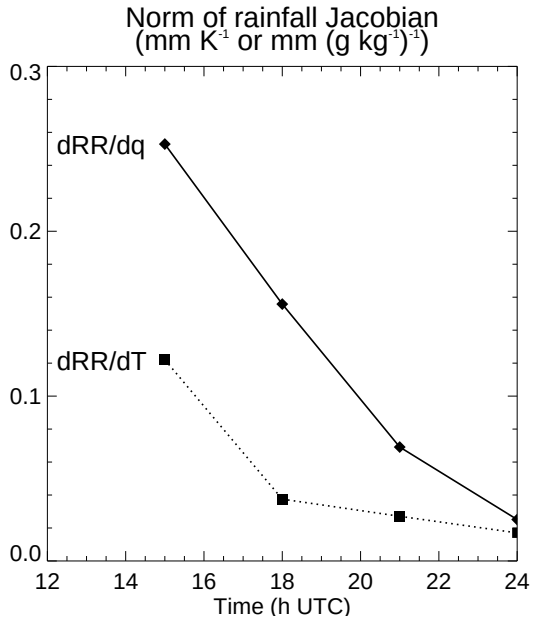

FIGURE 11: Time evolution of the norm of the Jacobians of *3-hourly accumulated rainfall* at the surface with respect to specific humidity (solid line) and temperature (dotted line) from experiment H_R4_GPS (see Table 2). For each time, the norm of the Jacobians with respect to a given variable is defined as their maximum absolute value in the vertical.

amount of rainfall since the comparison of Fig. 11 with Fig. 7.b shows that the Jacobians are strongest when the precipitation amount is low. In fact, the closer to the beginning of the assimilation window, the larger the impact of an initial perturbation of T or q on precipitation. This implies that when 2D-Var is used to assimilate several rainfall measurements in the same 12-hour window, earlier observations will tend to have more impact on the analysis than later ones. This can be understood by the fact that an increment in q applied at initial time while the model state is close to saturation is likely to be 'rained out' within the first time steps, thereby making any subsequent modification of precipitation impossible.

To investigate whether this issue could affect 4D-Var assimilation as well, adjoint sensitivities of 12-hour accu-

mulated surface rainfall to T and q perturbations with various lead times have been computed using a special configuration of the ECMWF model (Klinker *et al.* 1998). Compared to the original design, it is the use of the adjoint of the new simplified parametrizations of moist processes (Tompkins and Janisková 2004, Lopez and Moreau 2005) with their inclusion of precipitation perturbations that makes such calculations possible. Our purpose here is to check whether the three-dimensional sensitivities get lower when the lead time of the perturbation is increased. The computations of the nonlinear trajectory and of the adjoint evolution are performed at a T95 spectral resolution (200 km) and with 60 vertical levels.

The selected case is tropical cyclone Isabel in its mature stage north of the Lesser Antilles in mid-September 2003. Figure 12 displays the 12-hour accumulated surface precipitation and mean-sea-level pressure (MSLP) at 0000 UTC 13 September 2003 and at 1200 UTC 14 September 2003 from a forecast with the operational version of the ECMWF model started at 1200 UTC 12 September 2003. At 1200 UTC 14 September 2003, Isabel is located inside the black box shown on this map. The forecast aspect for which the sensitivities are to be computed is the 12-hour accumulated rainfall amount at 1200 UTC 14 September 2003 averaged over the box (denoted $< RR_{12h} >$) and it is equal to 4 mm. The maximum value over the 24 grid points located inside the target box reaches 8 mm in 12 hours, a very modest value that can be explained by the rather coarse horizontal resolution used here, as suggested by tests run with different resolution.

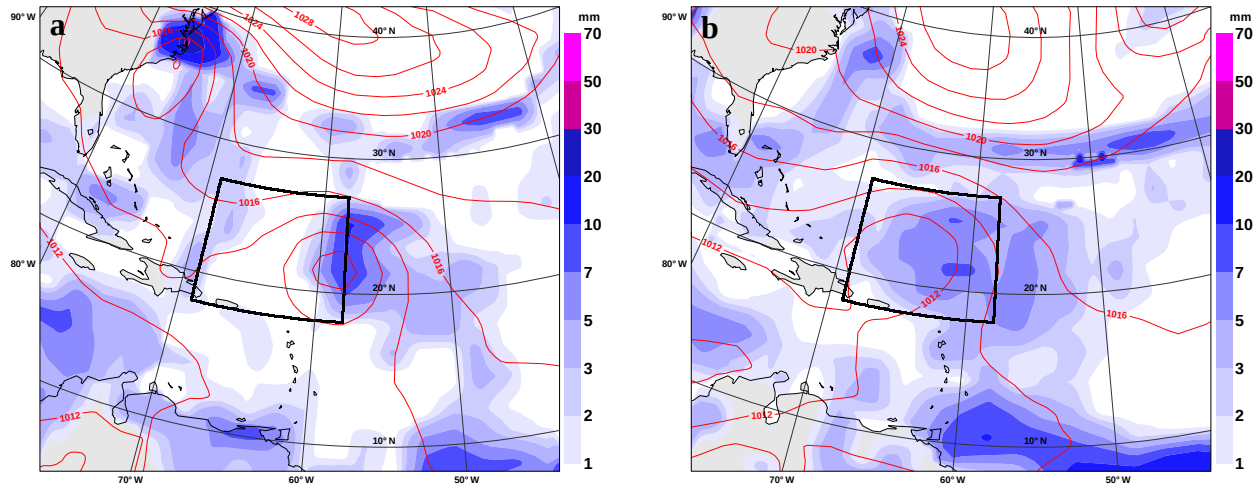

FIGURE 12: Tropical cyclone Isabel case: 12-hour accumulated surface rainfall (shading; in mm) and MSLP (isolines; every 2 hPa) at (a) 0000 UTC 13 September 2003 and (b) 1200 UTC 14 September 2003, from a T95 L60 integration started at 1200 UTC 12 September 2003.

An example of $\partial < RR_{12h} > /\partial T$ and $\partial < RR_{12h} > /\partial q$ is shown in Fig. 13 for perturbations applied on model level 50 (see Table 1) and at 0000 UTC 13 September 2003. Note that these sensitivities have been scaled to a 100 hPa-thick atmospheric layer so that their values at different vertical levels can be easily intercompared. As expected from the backward adjoint integration, the patterns of sensitivities to T and q are located upwind relative to the target box and to the prevailing mid-tropospheric easterly flow. $\partial < RR_{12h} > /\partial q$ is mainly positive which indicates that a moistening on model level 50 will result in enhanced surface precipitation one day later. $\partial < RR_{12h} > /\partial T$ exhibits a more marked bipolar pattern with positive values inside the storm's core and negative values around it. These sensitivities to temperature can be understood by realizing that a warming inside or a cooling outside the storm would both result in an intensification of the tropical cyclone's radial circulation and therefore lead to the release of more precipitation. For similar reasons, the sensitivities to temperature in the upper troposphere are opposite (not shown).

Figure 14 displays the time evolution of the vertical profiles of maximum absolute value of the rainfall sensitivities (obviously, the strongest sensitivities always occur not far away from the storm). Note that the 'lead times' on the x-axis are negative to denote the backward integration of the adjoint model and that lead time 0 corresponds to the beginning of the surface rainfall accumulation, that is 0000 UTC 14 September 2003. One should also keep in mind that in practice the sensitivities should be multiplied by typical values of T and q perturbations on each model level (Fig. 2) in order to obtain the actual resulting change in surface rainfall. Figure 14 shows that the longer the adjoint integration, the weaker the sensitivities of rainfall to T and q. This drop of the sensitivities is more pronounced between the surface and model level 52 and beyond 12 hours of adjoint backward integration. It is also sharper for the sensitivity to temperature than for that to specific humidity. For lead times less than 12 hours, the sensitivities are not as much reduced, especially with respect to moisture. This suggests that the uneven weighting of rain-gauge observations inside the assimilation window that is likely to occur in 2D-Var is less of a problem in 4D-Var, provided the length of the assimilation window does not exceed 12 hours. A likely explanation for these two different behaviours lies in the three-dimensional nature of the increments and their interaction with the dynamics in the 4D context, while the 2D-Var produces purely local increments of T and q that are completely independent from the SCM dynamical forcings. Therefore the 4D-Var assimilation of several co-located accumulated surface rain-gauge measurements within the 12-hour assimilation window should not be affected too much by the problem found in 2D-Var.

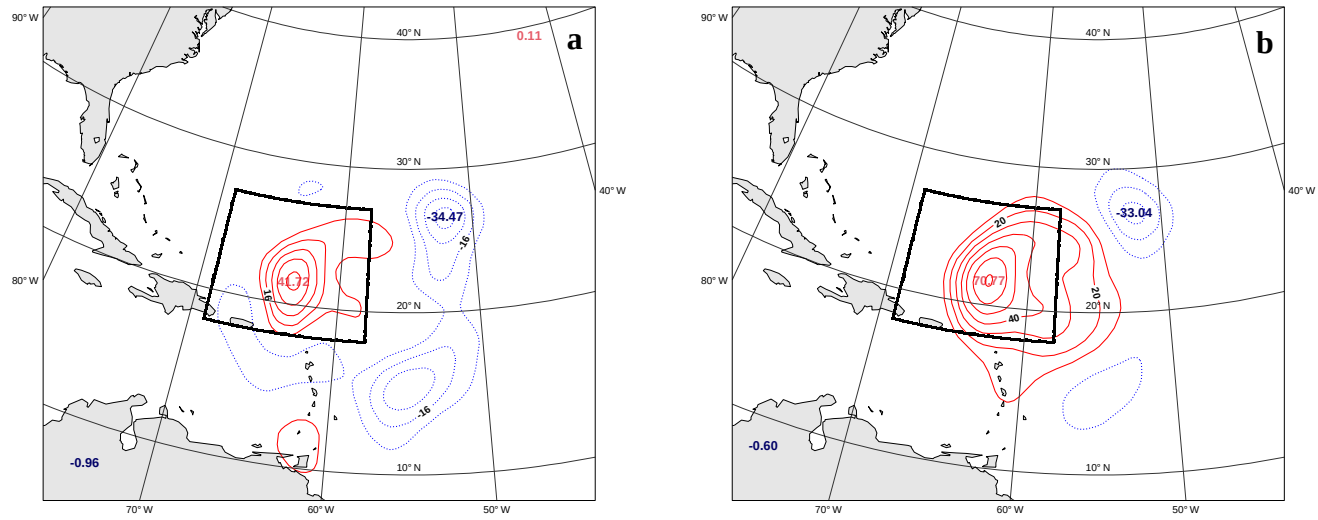

FIGURE 13: Tropical cyclone Isabel case: maps of sensitivities of the 12-hourly accumulated surface rainfall inside the target box (accumulation started at 0000 UTC 14 September 2003) with respect to (a) T and (b) q on model level 50 at 0000 UTC 13 September 2003. Sensitivities are in mm K^{-1} and mm $(g\ kg^{-1})^{-1}$ respectively and have been scaled to a 100 hPa-thick layer.

6 Conclusions

The purpose of this study was to identify the issues that are likely to be encountered in the future assimilation of observations that are directly affected by clouds and hydrometeors. The chosen 2D-Var framework facilitates the focus on the issues related to the inclusion of the temporal dimension in the minimization when several instantaneous observations or time-accumulated or time-averaged measurements are to be assimilated.

The first experiments run on ARM cloud-radar reflectivities have shown that the assimilation of half-hourly pro-

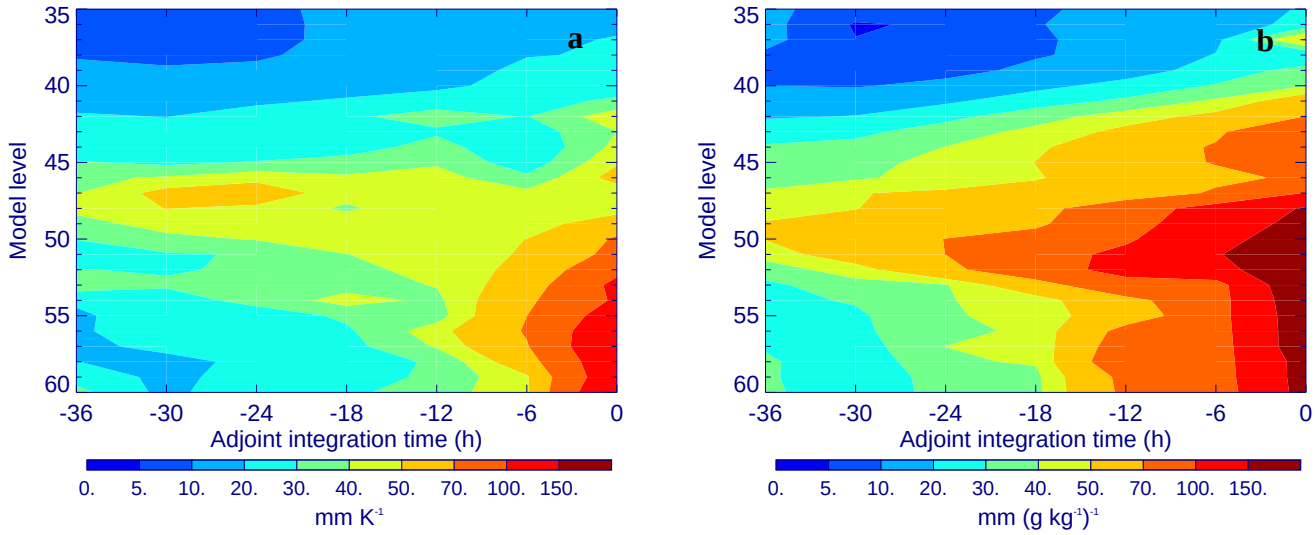

FIGURE 14: Tropical cyclone Isabel case: sensitivities of the 12-hourly accumulated surface rainfall inside the target box (accumulation started at 0000 UTC 14 September 2003) with respect to (a) T and (b) q up to 36 hours earlier. Lead times are in hours prior to 1200 UTC 14 September 2003.

files is problematic because of the large model−observation departures on such timescale. Proper convergence of the minimization can be obtained if a single profile of reflectivities averaged over the assimilation window is used instead. However, when the background reflectivities are much lower than observed, the required production of additional precipitation by the model can result in the non-convergence of the minimization because of the falling of these extra hydrometeors towards the surface. How acute this problem is depends on the treatment of precipitation in the model (diagnostic versus prognostic) as well as on the quality of the simulated humidity field that governs precipitation evaporation below cloud base. The assimilation of half-hourly microwave TBs from the ground-based radiometer turns out to be much less problematic because they are smoothly varying in time, even in cloudy conditions with no precipitation at the surface. In the future, combining time-averaged profiles of reflectivity with high-frequency (e.g. half-hourly) microwave TBs appears to be a suitable method for assimilating information on clouds. Furthermore, the assimilation of other statistical moments of reflectivities, such as their temporal variance, might be beneficial, but this will need to be tested.

Other experiments in precipitating cases have proven that the assimilation of accumulated rain-gauge measurements can lead to reasonable 2D-Var increments provided information on the moisture field (e.g. GPS data or radiosoundings) is also used to constrain the minimization. This latter condition is expected to be generally fulfilled in the context of 4D-Var. Similar results are obtained whether the minimization problem is solved by explicit computation of the Hessian or by using the M1QN3 iterative algorithm. It has been shown that the sensitivities of surface precipitation to the initial temperature and specific humidity profiles quickly decrease with the lead time of the T and q perturbations in the 2D-Var context. This implies that the respective weights of a set of asynchronous observations in the minimization is larger for those observations performed at the beginning of the assimilation window. However, three-dimensional adjoint computations of surface rainfall sensitivity to T and q have suggested that this problem should not be as critical in the current 12-hour assimilation window of 4D-Var. Indeed the inclusion of the horizontal dynamics in 4D-Var means that sensitivities can also arise from non-local perturbations, contrary to 2D-Var in which only local changes of initial T and q are considered.

Based on these results and given the fairly good coverage of real-time rain-gauge observations especially over Europe and North America, future efforts will be dedicated to investigate the possibility of assimilating (12-

hour) accumulated precipitation measurements directly into 4D-Var. To reach this goal, their representativeness will first need to be assessed, possibly using ground-based precipitation radar data to quantify their spatial variability, and their error statistics will need to be properly specified. Similar studies could focus on the assimilation of radar reflectivities or precipitation retrievals from existing ground-based precipitation radar networks, although real-time availability of such data could be more of an issue.

Acknowledgements

Jean-Noël Thépaut, Martin Miller, Anton Beljaars, Adrian Tompkins and Philippe Bougeault should be acknowlegded for reviewing this paper. We are very grateful to the ARM team for providing and carefully monitoring all the observations used in this study. The ARM Program is sponsored by the U.S. Department of Energy, Office of Science, Office of Biological and Environmental Research, Environmental Sciences Division. We would also like to thank INRIA (Institut National de Recherche en Informatique et en Automatique) for providing the M1QN3 minization code.

References

Bauer, P. (2001). Including a melting layer in microwave radiative transfer simulation for clouds. *Atmos. Research*, 57:9–30.

Bauer, P. (2002). Microwave radiative transfer modelling in clouds and precipitation. Part I: Model description. Technical report. Satellite Application Facility for Numerical Weather Prediction, NWPSAF-EC-TR-005, version 1.0.

Bechtold, P., Chaboureau, J.-P., Beljaars, A., Betts, A. K., Köhler, M., Miller, M., and Redelsperger, J.-L. (2005). The simulation of the diurnal cycle of convective precipitation over land in a global model. *Q. J. R. Meteorol. Soc.*, 131. in press.

Betts, A. K. and Jakob, C. (2002). Evaluation of the diurnal cycle of precipitation, surface thermodynamics, and surface fluxes in the ECMWF model using LBA data. *J. Geophys. Res.*, 107. (D20), 8045, doi:10.1029/2001JD000427.

Ducrocq, V., Ricard, D., Lafore, J.-P., and Orain, F. (2002). Storm-scale numerical rainfall prediction for five precipitating events over France: On the importance of the initial humidity field. *Weather Forecast.*, 17:1236–1256.

Gilbert, J.-C. and Lemaréchal, C. (1989). Some numerical experiments with variable-storage quasi-Newton algorithms. *Math. Programming*, 45:407–435.

Gregory, D. (2001). Estimation of entrainment rate in simple models of convective clouds. *Q. J. R. Meteorol. Soc.*, 127:53–72.

Hou, A. Y., Zhang, S. Q., and Reale, O. (2004). Variational continuous assimilation of TMI and SSM/I rain rates: Impact on GEOS-3 hurricane analyses and forecasts. *Mon. Weather Rev.*, 132:2094–2109.

Hou, A. Y., Zhang, S. Q., Silva, A. M. D., Olson, W. S., Kummerow, C. D., and Simpson, J. (2001). Improving global analysis and short-range forecast using rainfall and moisture observations derived from TRMM and SSM/I passive microwave sensors. *Bull. Am. Meteorol. Soc.*, 82:659–679.

Klinker, E., Rabier, F., and Gelaro, R. (1998). Estimation of key analysis errors using the adjoint technique. *Q. J. R. Meteorol. Soc.*, 124:1909–1933.

Lopez, P. (2003). The inclusion of 3D prognostic cloud and precipitation variables in adjoint calculations. *Mon. Weather Rev.*, 131:1953–1974.

Lopez, P. and Moreau, E. (2005). A convection scheme for data assimilation: Description and initial tests. *Q. J. R. Meteorol. Soc.*, 131. accepted.

Macpherson, B. (2001). Operational experience with assimilation of rainfall data in the Met.Office mesoscale model. *Meteorol. Atmos. Phys.*, 76:3–8.

Marécal, V. and Mahfouf, J.-F. (2002). Four-dimensional variational assimilation of total column water vapour in rainy areas. *Mon. Weather Rev.*, 130:43–58.

Marécal, V. and Mahfouf, J.-F. (2003). Experiments on 4D-Var assimilation of rainfall data using an incremental formulation. *Q. J. R. Meteorol. Soc.*, 129:3137–3160.

Moreau, E., Bauer, P., and Chevallier, F. (2003). Variational retrieval of rain profiles from spaceborne passive microwave radiance observations. *J. Geophys. Res.*, 203. (D16), 4521, doi: 10.1029/2002JD003315.

Moreau, E., Lopez, P., Bauer, P., Tompkins, A. M., Janisková, M., and Chevallier, F. (2004). Variational retrieval of temperature and humidity profiles using rain rates versus microwave brightness temperatures. *Q. J. R. Meteorol. Soc.*, 130:827–852.

Peng, S. Q. and Zou, X. (2002). Assimilation of NCEP multi-sensor hourly rainfall data using 4D-Var approach: A case study of the squall line on April 5, 1999. *Meteorol. Atmos. Phys.*, 81:237–255.

Rabier, F., McNally, A., Andersson, E., Courtier, P., Unden, P., Eyre, J., Hollingsworth, A., and Bouttier, F. (1998). The ECMWF implementation of the three dimensional variational assimilation (3D-Var). Part II: Structure functions. *Q. J. R. Meteorol. Soc.*, 124:1809–1829.

Stokes, G. M. and Schwartz, S. E. (1994). The Atmospheric Radiation Measurement (ARM) Program: programmatic background and design of the cloud and radiation test bed. *Bull. Am. Meteorol. Soc.*, 75:1201–1221.

Thurai, M., Kumagai, H., Kozu, T., and Akawa, J. (2001). Effects of incorporating a bright-band model in a downward looking radar rainfall retrieval algorithm. *J. Ocean. Atmos. Tech.*, 18:20–25.

Tiedtke, M. (1989). A comprehensive mass flux scheme for cumulus parameterization in large-scale models. *Mon. Weather Rev.*, 117:1779–1800.

Tiedtke, M. (1993). Representation of clouds in large-scale models. *Mon. Weather Rev.*, 121:3040–3061.

Tompkins, A. M. and Janisková, M. (2004). A cloud scheme for data assimilation: Description and initial tests. *Q. J. R. Meteorol. Soc.*, 130:2495–2518.

Tregoning, P., Boers, R., O'Brien, D., and Hendy, M. (1998). Accuracy of absolute precipitable water vapor estimates from GPS observations. *J. Geophys. Res.*, 103:28701–28710.

Ware, R. H., Fulker, D. W., Stein, S. A., Anderson, D. N., Avery, S. K., Clark, R. D., Droegemeier, K. K., Kuettner, J. P., Minster, J. B., and Sorooshian, S. (2000). SuomiNet: A RealTime National GPS Network for Atmospheric Research and Education. *Bull. Am. Meteorol. Soc.*, 81:677–694.